Earthquakes and Structures, *Vol. 17, No. 6 (2019) 599-609*
DOI: https://doi.org/10.12989/eas.2019.17.6.599

Post-earthquake assessment of buildings using displacement and acceleration response

Ting-Yu Hsu*[1,2] and Quang-Vinh Pham[1a]

[1]*Department of Civil and Construction Engineering, National Taiwan University of Science and Technology, Taipei, Taiwan*
[2]*Taiwan Building Technology Center, National Taiwan University of Science and Technology, Taipei, Taiwan*

(*Received July 3, 2019, Revised October 6, 2019, Accepted November 7, 2019*)

Abstract. After an earthquake, a quick seismic assessment of a structure can facilitate the recovery of operations, and consequently, improve structural resilience. Especially for facilities that play a key role in rescue or refuge efforts (e.g., hospitals and power facilities), or even economically important facilities (e.g., high-tech factories and financial centers), immediately resuming operations after disruptions resulting from an earthquake is critical. Therefore, this study proposes a prompt post-earthquake seismic evaluation method that uses displacement and acceleration measurements taken from real structural responses that resulted during an earthquake. With a prepared pre-earthquake capacity curve of a structure, the residual seismic capacity can be estimated using the residual roof drift ratio and stiffness. The proposed method was verified using a 6-story steel frame structure on a shaking table. The structure was damaged during a moderate earthquake, after which it collapsed completely during a severe earthquake. According to the experimental results, a reasonable estimation of the residual seismic capacity of structures can be performed using the proposed post-earthquake seismic evaluation method.

Keywords: capacity assessment; damage detection/assessment; earthquake/seismic response; residual displacement; stiffness degradation

1. Introduction

Resilience from a catastrophic earthquake is affected not only by pre-disaster mitigation but also by society's ability to mute post-event losses and recover rapidly from such an event. A key characteristic of disaster-resilient communities is that such communities experience minimum disruption to life and their economy after a hazard event (NRC 2011). During a catastrophic earthquake, hundreds of thousands of buildings could incur damage. When such a massive quantity of buildings sustains sudden damage, at least several months are required to send engineers on site to evaluate the remaining seismic capacity, based mainly on subjective visual examinations, with little support from objective engineering values. Moreover, to conduct an in-situ assessment of the damaged buildings, engineers are assuming considerable risk entering damaged buildings because of dangerous aftershocks. Recent studies showed that structures with residual deformation under the main shock may greatly affect the seismic performance and lead to severe damage or collapse during the occurrence of aftershocks (Ruiz-García and Aguilar 2014, Tang *et al*. 2016, Kostinakis and Morfidis 2017, Li *et al*. 2017). Therefore, a fast, safe, and unbiased seismic evaluation is warranted.

The seismic capacity of buildings can be evaluated using analytical procedures. Because the structural response of buildings to strong ground motions results in inelastic behavior, a nonlinear analytical approach is required. Although a nonlinear dynamic analysis is believed to be the most powerful tool for predicting the actual response of a building, it necessitates high computational resources. By contrast, nonlinear static pushover analysis is an efficient method for predicting the seismic behavior of structures with the fundamental first mode. This method has been widely applied to practical seismic assessments of buildings, and is available in publications such as the ATC-40 report (1996), the ASCE 41 report (2007), FEMA 273 (1997), and FEMA 356 (2000). The capacity spectrum method (CSM), presented in the ATC-40 report, has been adopted in performance-based seismic evaluations and accepted by practical engineers. However, deficiencies in the CSM still persist. Therefore, Sung (2003) proposed a modified CSM, which can evaluate the full range of the corresponding seismic demand. It calculates the demand spectrum by defining the performance point of the structure corresponding to the ultimate seismic capacity. The modified CSM became highly efficient because iterations are unnecessary, and it has been employed successfully to bridge structures (Sung 2003) and low-rise buildings (Sung *et al*. 2006, Hsiao *et al*. 2016).

The traditional evaluation approach for the seismic capacity of a building damaged during an earthquake requires that engineers gather information by conducting an in-situ examination. If a component is damaged, based on the expert judgment of engineers, the stiffness or capacity value of that component may be reduced before nonlinear

*Corresponding author, Assistant Professor
E-mail: tyhsu@ntust.edu.tw
[a]Graduate Student
E-mail: quangvinhphamhau@gmail.com

ISSN: 2092-7614 (Print), 2092-7622 (Online)

static pushover analysis is performed. Post-earthquake damage assessment could also be performaed based on residual drift measured in-situ (Dai *et al*. 2017). However, obtaining this in-situ information is time-consuming, subjective, and dangerous.

Another potential solution is to install adequate sensors on the building and record the necessary seismic response of the building during an earthquake. By doing so, the building can be seismically evaluated using objective scientific values immediately after an earthquake, without risking the safety of engineers. Thanks to the rapid development of sensor technology over the past decade, the cost of sensors is decreasing and becoming reasonably priced for large-scale installation on buildings. One successful employment of sensors for detecting damage in a building during an earthquake concerns the use of the inter-story drift ratio (IDR) and related fragility curves (Naeim *et al*. 2005). The health condition of the building (i.e., non-damage, slightly damage, moderate damage, and severe damage) can be assessed. However, the remaining seismic capacity of the building remains unknown. On the other hand, Dunand *et al*. (2004) proposed to use measurement data to assess earthquake-damaged buildings. Ozer and Soyoz (2013) evaluated the residual capacity of earthquake-damaged reinforced-concrete bridge columns through updated fragility curves. Trevlopoulos and Gueguen (2016) proposed to use measured period elongation to evaluate vulnerability through a sequence of aftershocks. Reuland *et al*. (2019) tried to combine visual inspection and modal measurements to assess earthquake-damaged structures.

In actuality, not only structural health monitoring but also a seismic evaluation could benefit from structural responses as measured by sensors. This study proposes employing measured building responses during an earthquake to perform post-earthquake seismic capacity estimations. To evaluate the seismic capacity of a building immediately after an earthquake using the measured response, nonlinear static pushover analysis prior to an earthquake is required. The remainder of this study is organized as follows: Section II details the proposed methodology; Section III presents an experiment involving a shaking table test with a 6-story steel building, which was conducted to verify the proposed approach; Section IV provides the results; and lastly, Section V offers a discussion and conclusion.

2. Methodology

Although accelerometers are readily purchasable, commercial products for measuring inter-story drift are relatively rare, albeit not unavailable. Therefore, in this study, we assume that the relative displacement and absolute acceleration of a building response of each story during an earthquake can be measured simultaneously with acceptable accuracy. In addition, nonlinear static pushover analysis is a requirement that is assumed possible to conduct when the building is intact. We propose employing the measured building responses to perform post-earthquake seismic capacity estimations by using the reduction of stiffness and maximum residual roof displacement as 2 key parameters.

The time history of the relative roof displacement of building Δ_R at time t_k can be calculated by summing the relative displacement of each floor

$$\Delta_R(t_k) = \sum_{j=1}^{N} d_j(t_k) \tag{1}$$

where d_j represents the time history of the inter-story drift of the jth story, and N represents the total number of stories. For a real building, measuring the base shear V is not easy. Alternatively, one can use the following equation to calculate the time history of the estimated base shear of building V_e, using the measured absolute acceleration and lumped mass of each floor

$$V_e(t_k) = \sum_{j=1}^{N} m_j \ddot{x}_j(t_k) \tag{2}$$

where m_j and $\ddot{x}_j$ represent the lumped mass and the time history of absolute acceleration of the jth floor, respectively. The ground floor is not included in this equation. The estimated base shear can be normalized by dividing it by the total weight, as follows

$$V_n(t_k) = V_e(t_k) \Big/ \sum_{j=1}^{N} m_j g \tag{3}$$

where V_n represents the normalized estimated base shear, and g denotes the gravitational acceleration. The normalized residual stiffness (i.e., normalized estimated base shear per relative roof displacement) of the building during an earthquake can be estimated using the curve-fitting approach. Because of the potential for a low signal-to-noise ratio (SNR) of the measured acceleration response during a smaller ground vibration in the tail of an earthquake, a suitable range of amplitude of the acceleration response is required to determine the normalized residual stiffness when the structural behavior is linear.

The upper bound of the range depends on not only the building types, but also the seismic demand of the location of the building. The consequence of these two factors is the normalized seismic design base shear of the building. Therefore, the upper bound of the range is mainly dependent on the structural normalized seismic design base shear. A higher normalized seismic design base shear should guarantee a linear behavior for the structure during a larger ground excitation, whereas the structure begins assuming a nonlinear behavior much earlier with a low seismic design level. The upper bound of 75 Gal is suitable for the buildings in Taiwan. For the building in a different location, the upper bound should be considered based on the seismic design results. Conversely, the lower bound is mainly dependent on the capability of the measurement system. A smaller lower bound can be used with a higher-performing measurement system. Therefore, the range is not identical for every case.

In this study, the range was set from 25 to 75 Gal for the measured roof acceleration response. The lower bound was set at 25 Gal because the hysteretic diagram is dispersed when the measured roof acceleration response is lower than this value. The upper bound was set to 75 Gal because a sufficient amount of linear data was available for use to

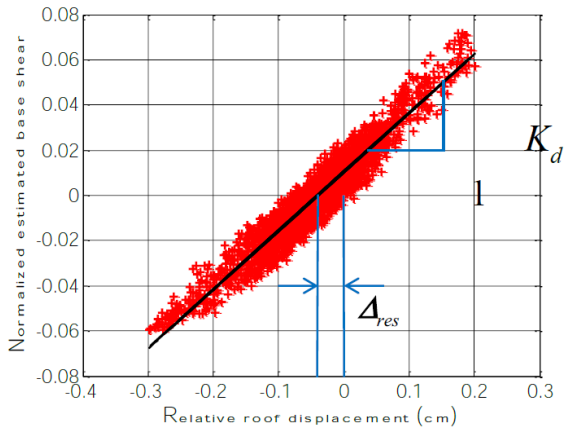

Fig. 1 Typical results of the estimated normalized residual stiffness and maximum residual roof displacement

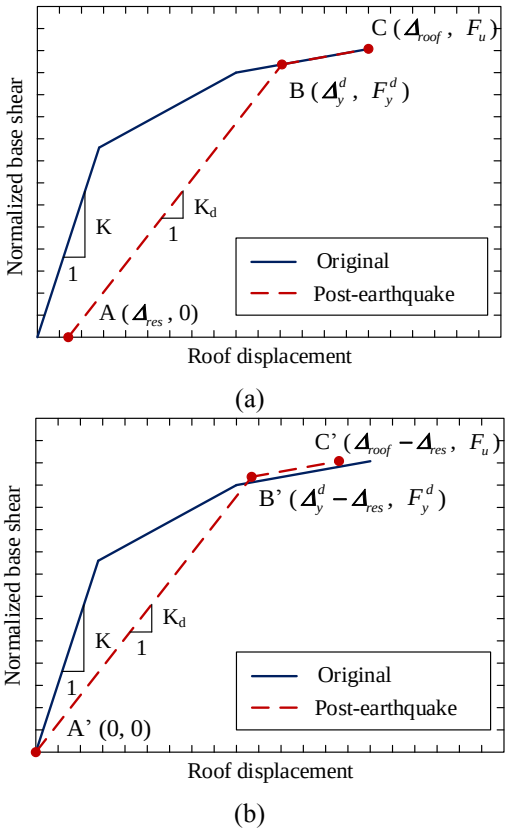

Fig. 2 Procedures for estimating post-earthquake seismic capacity using the estimated normalized residual stiffness and maximum residual roof displacement based on the original seismic capacity curve. (a) Step 1 and (b) Step 2

estimate the normalized residual stiffness for all the studied ground excitations. The normalized residual stiffness is estimated through curve fitting by solving the first-degree polynomial equation. Once the normalized residual stiffness is determined, the maximum residual roof displacement, Δ_{res}, can be estimated for use as the intercept (Fig. 1). In a number of cases, the residual displacement estimated using the tail of the time history of an earthquake response can potentially be smaller than the other residual displacement during the same earthquake. For such cases, the maximum residual displacement should be estimated using the corresponding linear response, after which it can be used to estimate the post-earthquake seismic capacity.

The post-earthquake seismic capacity can be estimated using normalized residual stiffness K_d and maximum residual displacement Δ_{res}. (The procedures are displayed in Fig. 2). The estimation procedure begins by drawing a line with the normalized residual stiffness from the point with the maximum residual displacement and the zero base shear (i.e., point A in Fig. 2(a)) to identify the first intersection with the original capacity curve (i.e., point B in Fig. 2(a)). The coordinates of point A and point B are (Δ_{res}, 0) and B (Δ_y^d, F_y^d), respectively. Afterward, the remaining part of the post-earthquake capacity curve follows the original capacity curve after intersection point B, until the roof displacement is equal to the ultimate roof displacement Δ_{roof} (i.e., point C) (Fig. 2(a)). The coordinate of point C is C (Δ_{roof}, F_u), where F_u is the ultimate normalized base shear.

Next, lines AB and BC are shifted by reducing the displacement by Δ_{res} to start from the original point, after which the post-earthquake capacity curve is obtained (i.e., line A'B'C', as shown in Fig. 2(b)). When the estimated residual stiffness is small and the maximum residual displacement is large, there is a possibility that no intersection may occur with the original capacity curve because the roof displacement is limited.

Once the capacity curve is obtained, it is possible to perform a post-earthquake seismic evaluation of the structure by using the modified CSM (Hsiao *et al*. 2016).

In this study, all the points in the capacity curve were treated as performance points and used to calculate the corresponding seismic demand. By employing these predetermined performance points and following the ATC-40 procedure to obtain the equivalent capacity spectrum, the effective damping β_{eq} can be calculated based on a bilinear simplification of the capacity spectrum and a designated reasonable damping modification factor κ. Finally, the capacity, as determined by referring to the peak ground acceleration (PGA) value, can be calculated based on (4) to (7). The parameters of the seismic design spectrum used in this study was following Taiwan's seismic design code (CPAMI 2011).

$$A_p = \frac{S_{a,p}}{\left[1+\left(\frac{2.5}{B_s}-1\right)\frac{T_{eq}}{0.2T_0}\right]} \quad \text{for} \quad T_{eq} \le 0.2T_0 \tag{4}$$

$$A_p = \frac{B_s}{2.5} S_{a,p} \quad \text{for} \quad 0.2T_0 < T_{eq} \le T_0 \tag{5}$$

$$A_p = \frac{B_s T_{eq}}{2.5T_0} S_{a,p} \quad \text{for} \quad T_0 < T_{eq} \tag{6}$$

$$T_{eq} = 2\pi\sqrt{\frac{d_p}{a_p g}} \tag{7}$$

where A_p represents the seismic capacity (PGA) of the structure in the predetermined performance point; B_s and B_l represents the correction factors; and $S_{a,p}$ denotes the

spectral acceleration of the predetermined performance point. Finally, T_{eq} denotes the fundamental period corresponding to the predetermined performance point (d_p, a_p), where d_p and a_p represent spectral displacement and spectral acceleration, respectively, in the predetermined performance point. T_0 denotes the characteristic period defined as $T_0 = (S_{D1}B_s)/(S_{DS}B_l)$, where S_{D1} and S_{DS} depict spectral acceleration at 1.0 s and maximum spectral acceleration, respectively, in the 5% damped spectrum. In this study, S_{D1} and S_{DS} were equal to 0.45 g and 0.8 g, respectively, and κ was equal to 0.67 considering the hysteretic loops under the capacity curve was not perfect. For all the cases examined, the performance point at the maximum roof displacement was found to have the maximum seismic capacity of a building. Therefore, the maximum seismic capacity (PGA), when the structure is intact as well as after an earthquake, was designated A_p^I and A_p^D, respectively. The residual seismic capacity ratio of the structure is defined as

$$R_c = \frac{A_p^D}{A_p^I} \times 100\% \tag{8}$$

3. Experimental program

3.1 Test structure description

A 1/3-scale 6-story steel structure constructed at the National Center for Research on Earthquake Engineering (NCREE), Taiwan, was used to experimentally validate the proposed method. As shown in Fig. 3, the structure consisted of a single bay comprising a 1.1 m×1.5 m floor area, with a uniform height of 1.18 m per story. The cross-section of the beams was 50 mm×100 mm×6 mm (U-section). Due to budget limitations, the upper 3 stories of the steel building were loaned from another project.

The overall stiffness and strength of these 3 upper stories were much higher compared to their 3 lower counterparts. The cross-section of the columns and bracings of these upper stories measured 150 mm×25 mm (rectangular section) and 65 mm×65 mm×6 mm (L-section), respectively. To confirm that the steel building would sustain damage during the shaking table test, the structure was designed to have less seismic capacity in the lower three stories. The cross-section of the lower columns was 100 mm×30 mm×5 mm×7 mm (H-section). In addition to the L-shaped bracings used in the upper stories, two differently sized tube bracings were used in the *x*-direction in the lower three stories. The outer diameter of these bracings measured 18 mm and 21.7 mm, respectively, with a thickness of 1.2 mm and 2 mm, respectively. For the entire steel building, the beam-floor connections were welded, whereas the beam-column connections and the base-column connections were bolted. The dead load was simulated with lead block units fixed to the steel plate of each floor. The total mass of each floor of the target structure was approximately 962.85 kg, except for the mass of the roof floor, which weighed 903.98 kg.

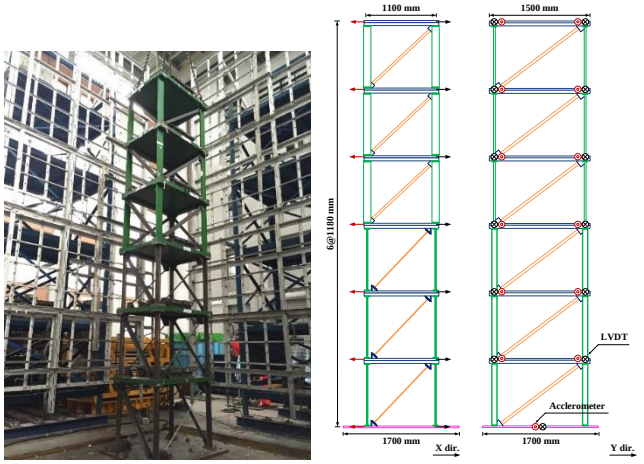

(a) (b)

Fig. 3 The 1/3-scale 6-story steel structure. (a) Overview and (b) plane views with sensor arrangement

Table 1 Bracing configuration of the 4 specimens

Specimen Designation	Story					
	1	2	3	4	5	6
A	*T*1	*T*2	*T*2	L	L	L
B	*T*1	*T*1	*T*2	L	L	L
C	*T*1	*T*1	*T*2	L	L	L
D	*T*1	*T*1	*T*2	L	L	L

3.2 Damage cases

Shaking table tests were performed for 4 specimens with various configurations of bracings and excitations. For all 4 specimens, the cross-section of all the bracings in the *y*-direction was of the L-section (labeled "*L*"), because the excitation of the shaking table occurred only in the *x*-direction, with the El Centro earthquake as input. For specimen A, only the first story was installed with the small tube bracing (labeled "*T*1"), with the larger tube bracings (labeled "*T*2") installed in the other 2 stories among the 3 lower stories.

PGA began at 50 Gal and increased by 50 Gal with each iteration, until it reached 350 Gal. We expected the damage to be concentrated in the first story because the seismic capacity of that story was smallest and the story shear was largest. The same sequence of excitations was conducted for specimen *B*, but the cross-section of the bracing in the second story was modified to *T*1. For specimens *C* and *D*, the bracing configuration was identical to that of specimen *B*. The only difference was the program of excitations, where only PGA values equal to 200 Gal, 300 Gal, and 350 Gal were inputted to specimen *C*, whereas PGA values of 250 Gal and 350 Gal were inputted to specimen *D* to investigate the residual seismic capacity after moderate earthquakes. The bracing configuration of the specimens is presented in summary form in Table 1.

3.3 Measurement

Two accelerometers in the x-direction were installed on

each side of each floor, and only one accelerometer was installed on the ground. The linear variable differential transformer (LVDT) facing the opposite *x*-direction was installed at the same locations of the accelerometers (Fig. 3). The sampling rate for discrete data collection was 200 Hz, with an earthquake duration of 46.08 s. The acceleration responses of each story were obtained by averaging the measured responses in the *x*-direction at both sides. Furthermore, to observe the buckling behavior caused by earthquake excitations, the lateral residual displacement in the middle of the bracing on the first story was monitored using a 3D optical displacement measurement system.

4. Experimental results

4.1 Nonlinear static pushover analysis

To obtain the capacity curve of the 6-story steel building specimens before excitation, we conducted nonlinear static pushover analysis by using the Platform of Inelastic Structural Analysis for 3D Systems (PISA3D) software, as developed by the NCREE (Lin and Tsai 2003, Lin *et al.* 2009). The elastic modulus, Poisson's ratio, and the density of the numerical model were 2.0×10^{11} N/m^2, 0.33, and 7.8×10^3 kg/m^3, respectively. The plastic hinge of the column element was assigned as a bilinear model at both ends, and the strain hardening ratio and the yielding stress of the column elements were 0.02 and 3.50×10^8 N/m^2, respectively. The bracings were designated predefined buckling materials in PISA3D with buckling stress 1.53×10^8 N/m^2. No plastic hinge was assigned in the beams because the beam was connected to the deck with lead blocked installed.

We increased the roof displacement incrementally until the IDR of any one of the stories reached their respective limit. The IDR limit was assigned according to the complete damage stage, as defined by the Federal Emergency Management Agency Hazus-MH 2.1 Earthquake Model Technical Manual (FEMA 2015). According to the manual, for a midrise steel-braced frame building with a high-code seismic design level, the IDR threshold for a complete structurally damaged state is 5.33%. The roof displacement at this stage (i.e., any story that has reached its limit) is defined as Δ_{roof}, at which point pushover analysis ends.

4.2 Calculation of seismic capacity

The capacity curve between the base shear and roof displacement was used to calculate the maximum seismic capacity (i.e., A_p^I) by using (4) to (7). Because the amplitude of the compression force for the bracings to buckle was much smaller than the tension force for the bracings to yield, during the darthquake, the brackings always buckled. Once the bracings were buckled, the direction to buckle the bracings became the much weaker than the opposite direction. As a result, the building always collapsed in the compression direction. Therefore, for conservation consideration, we estimated seismic capacities when the structure was intact as well as post-earthquake

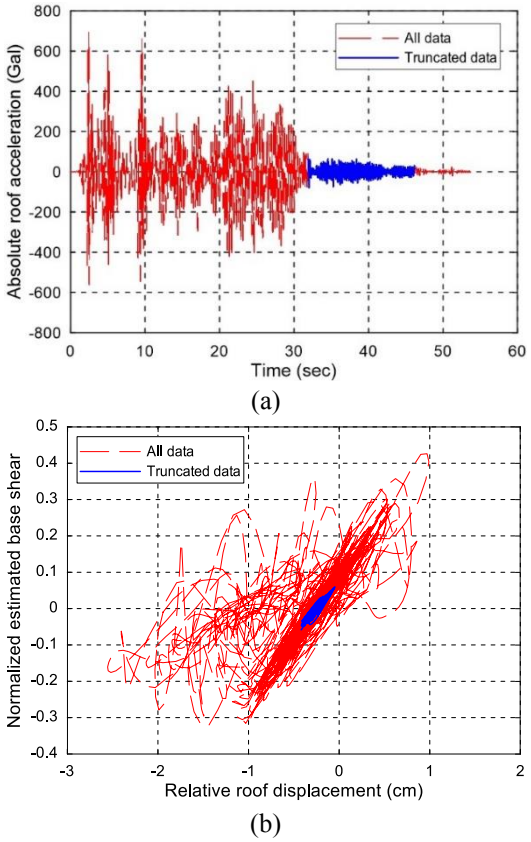

Fig. 4 Tytpilca structural response of the PISA3D model of Case 1 with PGA 250 Gal. (a) Time history of absolute roof acceleration and (b) hysteretic diagram of relative roof displacement and the estimated normalized base shear

were determined using the capacity curves in the compression direction.

4.3 Time history analysis

In order to validate the proposed approach to estimate the residual stiffness and the residual displacement, the time history analysis of the PISA3D model of Case 1 under the same earthquake excitations as the experimental tests were conducted. The results obtained by the proposed method are compared to the ones obtained using the analytical values of the total base shear and the roof displacement. The typical time history of absolute roof acceleration under PGA 250 gal is shown in Fig. 4(a). Fig. 4(b) displays the corresponding hysteretic diagram of relative roof displacement and estimated base shear. Apparently, the model behaves nonlinearly during this earthquake excitation. As indicated in these figures with a blue solid line, the last segment with a roof acceleration amplitude between 75 and 25 Gal was truncated to estimate the residual stiffness and residual roof displacement. The estimated residual stiffness was 1669.9 kN/m while the analytical stiffness was 1810.2 kN/m, i.e. the error of the estimated residual stiffness was approximately only 7.7%. The estimated residual roof displacement was -0.246 cm while the analytical one was also -0.246 cm, which is very close. Note that the residual stiffness after buckling of the

Table 2 Summary of the results of estimated residual stiffness and displacement

PGA (gal)	Residual stiffness K_d (kN/cm)			Residual drift for the roof Δ_{res}^{roof} (cm)		
	Estimated	Real	Error (%)	Estimated	Real	Error (cm)
50	1727.1	1810.2	-4.6	0.001	0.000	0.001
100	1755.6	1810.2	-3.0	0.000	0.000	0.000
150	1922.7	1810.2	6.2	-0.222	-0.222	0.000
200	1653.9	1810.2	-8.6	-0.452	-0.452	0.000
250	1669.9	1810.2	-7.8	-0.246	-0.246	0.000
300	1718.2	1810.2	-5.1	-1.934	-1.934	0.000

bracings and the yielding of the columns remained the same as the initial stiffness in the PISA3D model. Although this phenomenon was not the same as the real case, we can still understand the accuracy of the estimated parameters by comparing it to the analytical values. The results under different earthquake excitations were summarized in Table 2. The errors of the estimated residual stiffness were between -8.6% and 6.2%, whereas the ones of the estimated residual roof drift were close to 0 cm. Based on the results, the proposed method was verified to be able to estimate the residual stiffness and the residual displacement with acceptable error.

4.4 Observation of the experimental results

For specimen A, where only the first story was installed with small tube bracings, the originally estimated seismic capacity was 255.5 Gal. The capacity curves obtained from when the structure was intact are shown in Fig. 5. The time history of absolute roof acceleration during an earthquake with a PGA of 50 Gal is shown in Fig. 6(a). Fig. 6(b) displays the hysteretic diagram of relative roof displacement and estimated normalized base shear. As indicated in these figures with a blue solid line, the last segment with a roof acceleration amplitude between 75 and 25 Gal was truncated to estimate the residual stiffness and residual roof displacement. The post-earthquake capacity curve under compression is shown in Fig. 7. After the earthquake, the final post-earthquake seismic capacity A_p^D, calculated using (10), was 254.7 Gal, which is nearly identical to the value of the original seismic capacity A_p^I. The residual seismic capacity R_c was 99.7%; therefore, this indicated that the seismic capacity was well preserved. The residual stiffness ratio was calculated as

$$R_k = \frac{K_d}{K} \times 100\% \tag{9}$$

where K and K_d represent the intact and damaged normalized original stiffness, respectively. The calculated R_k was equal to 91.4%; therefore, approximately 10% of the stiffness decreased. The residual drift ratio for the first story and for the roof (i.e., Δ_{roof} divided by building height) was only 0.02% and 0.00%, respectively; therefore, barely any residual inter-story drift was observed. The residual lateral displacement in the middle of the bracing measured only

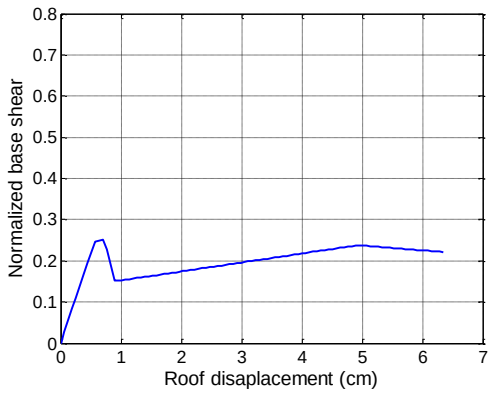

Fig. 5 Intact seismic capacity curves of specimen A when bracings are under compression

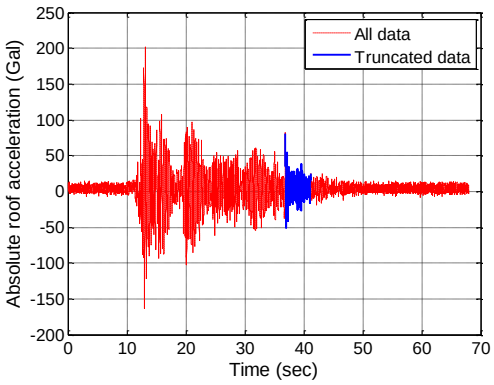

(a)

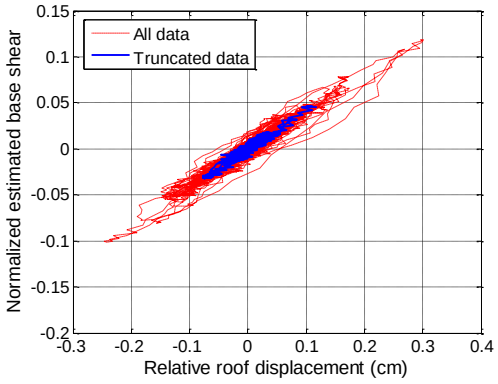

(b)

Fig. 6 Structural response of specimen A during an earthquake with a PGA of 50 Gal. (a) Time history of absolute roof acceleration and (b) hysteretic diagram of relative roof displacement and the estimated normalized base shear

0.03 cm. After a careful survey of the structure after the earthquake, we compared the findings against the description of the damaged states of different damage levels for the type "steel-braced frame" in the Hazus-MH 2.1 Earthquake Model Technical Manual; we designated the structural state as having sustained "no damage."

Following the same procedure, we obtained the results of specimen A after earthquake excitation with a PGA of 100 Gal and greater (Table 3). The post-earthquake seismic capacity, residual seismic capacity ratio, and residual drift

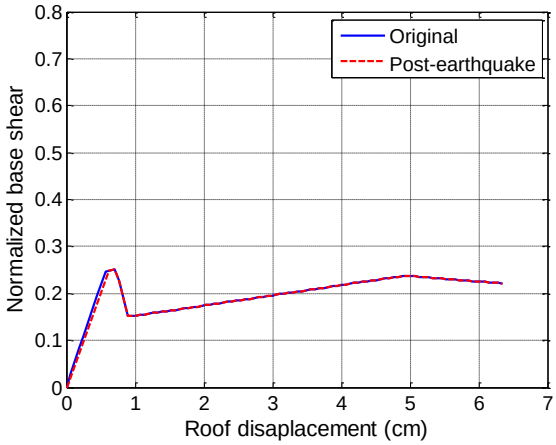

Fig. 7 Post-earthquake seismic capacity curves of specimen A when bracings are under compression after earthquake excitation with a PGA of 50 Gal

ratios after the PGA reached 100 Gal were nearly identical to the same specimen with a PGA of 50 Gal, except that the residual stiffness ratio decreased to 84.5% and the residual lateral displacement in the middle of the bracing increased to 0.63 cm. We concluded that the damaged state suffered "slight structural damage" because we identified a minor buckle for the bracings in the first story. After the PGA reached 150 Gal, the reduction in post-earthquake seismic capacity and the residual seismic capacity ratio as well as an increase in residual drift ratios continued to progress slightly. The residual stiffness ratio decreased to 63.2%, and the residual lateral displacement in the middle of the bracing increased to 2.23 cm. We therefore concluded that the damaged state suffered "moderate structural damage" because we could easily discern the buckle for the bracings in the first story. These damage indicators continued to progress as the PGA of the earthquake excitations increased to 250 Gal-except that the damaged state did not exceed its "moderate structural damage" designation. Although the stiffness reduction ratio increased to 31.0%, the residual seismic capacity ratio decreased only to 88.5%. The post-earthquake seismic capacity decreased to 226.2 Gal after the earthquake excitation with a PGA of 250 Gal. Fig. 8(a) shows the time history of absolute roof acceleration when the PGA increased to 300 Gal (i.e., larger than 226.2 Gal), and Fig. 8(b) displays the hysteretic diagram of the relative roof displacement and estimated normalized base shear for the same PGA value. The post-earthquake capacity curve under compression is shown in Fig. 9. The estimated post-earthquake seismic capacity, residual seismic capacity ratio, and residual stiffness ratio decreased substantially, to 64.2 Gal, 25.1%, and 11.7%, respectively. By contrast, the residual drift ratio of the first story and of the roof increased considerably to 0.74% and 4.53%, respectively, and the residual lateral displacement in the middle of the bracing also increased to 11.5 cm. We concluded that the entire structure suffered "extensive structural damage" because we observed a significant permanent lateral deformation in the structure. Finally, the specimen collapsed completely when the PGA reached 350 Gal.

We found the estimated post-earthquake seismic

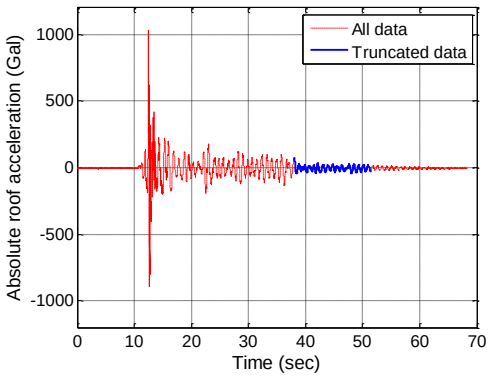

(a)

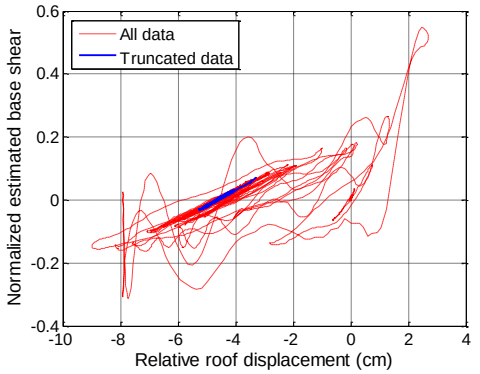

(b)

Fig. 8 Structural response of specimen A during an earthquake with a PGA of 300 Gal. (a) Time history of absolute roof acceleration and (b) hysteretic diagram of relative roof displacement and the estimated normalized base shear

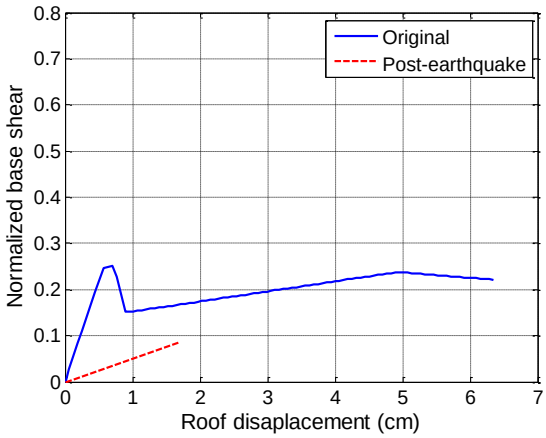

Fig. 9 Post-earthquake seismic capacity curves of specimen A when bracings are under compression after earthquake excitation with a PGA of 300 Gal

capacities of specimen A to be quite reasonable: They were larger than the excited PGA until Test No. 6, and the residual seismic capacity ratios remained relatively high (i.e., larger than approximately 88.5%) for the first 5 tests. For Test No. 6 with a PGA of 300 Gal, the estimated seismic capacity was 226.2 Gal prior to earthquake excitation. After the test, only 64.2 Gal remained in terms of the estimated post-earthquake seismic capacity. The residual

Table 3 Results of specimen A after earthquake excitation

No. of tests	Excited PGA (Gal)	Estimated seismic capacity A_p^D (Gal)	Residual seismic capacity ratio R_c (%)	Residual stiffness ratio R_k (%)	Residual drift ratio for the first story Δ_{res}^{1st} (%)	Residual drift ratio for the roof Δ_{res}^{roof} (%)	Residual lateral displacement of bracing (cm)	Observed damage level
1	50	254.7	99.7	91.4%	0.02	0.00	0.03	None
2	100	253.5	99.2	84.5%	0.05	0.00	0.63	Slight
3	150	247.9	97.0	63.2%	0.24	0.03	2.23	Moderate
4	200	247.0	96.7	56.6%	0.24	0.04	2.50	Moderate
5	250	226.2	88.5	31.0%	0.49	0.09	4.60	Moderate
6	300	64.2	25.1	11.7%	4.53	0.74	11.5	Extensive
7	350	Collapse						

Table 4 Results of specimen B after earthquake excitation

No. of tests	Excited PGA (Gal)	Estimated seismic capacity A_p^D (Gal)	Residual seismic capacity ratio R_c (%)	Residual stiffness ratio R_k (%)	Residual drift ratio for the first story Δ_{res}^{1st} (%)	Residual drift ratio for the roof Δ_{res}^{roof} (%)	Residual lateral displacement of bracing (cm)	Observed damage level
1	50	259.1	99.8	93.8	0.02	0.00	0.00	None
2	100	258.6	99.6	89.9	0.03	0.00	0.00	None
3	150	256.2	98.7	80.9	0.14	0.01	1.30	Moderate
4	200	254.8	98.2	70.3	0.19	0.01	2.20	Moderate
5	250	248.8	95.8	48.1	0.24	0.02	3.70	Moderate
6	300	132.0	50.8	14.3	2.49	0.38	9.60	Extensive
7	350	Collapse						

Table 5 Results of specimen C after earthquake excitation

No. of tests	Excited PGA (Gal)	Estimated seismic capacity A_p^D (Gal)	Residual seismic capacity ratio R_c (%)	Residual stiffness ratio R_k (%)	Residual drift ratio for the first story Δ_{res}^{1st} (%)	Residual drift ratio for the roof Δ_{res}^{roof} (%)	Residual lateral displacement of bracing (cm)	Observed damage level
1	200	250.8	96.6	58.6	0.24	0.04	2.90	Moderate
2	300	91.3	35.2	13.6	4.22	0.70	13.5	Extensive
3	350	Collapse						

drift ratio for the first story reached 4.53%, which was close to 5.33%, a value that was used as the maximum story drift ratio in pushover analysis, and then the structure collapsed in the subsequent test.

For specimen B, where only the first 2 stories were installed with the small tube bracings, the original estimated seismic capacity was 259.6 Gal, which was slightly larger than that of specimen *A* (i.e., 255.5 Gal), because the damage would not be as concentrated to the first story as in specimen *A*. Following the same procedure, we obtained the results of specimen *B* after various earthquake excitations (Table 4). The test procedures were identical to those for specimen *A*, and the results were generally quite similar to those obtained for that specimen. We again found the estimated post-earthquake seismic capacities to be quite reasonable. For Test No. 6, the estimated seismic capacity was 248.8 Gal prior to earthquake excitation, and the residual drift ratio for the first story reached 2.49%, which was approximately half of 5.33%, a value that was used as the decisive story drift ratio in pushover analysis. The remaining estimated post-earthquake seismic capacity was only 132.0 Gal after the test, with an excited PGA of 300 Gal. The structure collapsed in the subsequent test.

For specimen *C*, which is identical to specimen *B*, we obtained the results after different earthquake excitations (Table 5). After the first test, when the PGA reached 200 Gal, the estimated post-earthquake seismic capacity was 250.8 Gal, and the residual seismic capacity ratio was 96.6%. The residual drift ratio of the first story and the roof was only 0.24% and 0.04%, respectively; thus, the residual inter-story drift could not be observed easily. The residual stiffness ratio was 58.6%, and the residual lateral displacement in the middle of the bracing measured 2.90 cm. We concluded that the entire structure suffered "moderate structural damage" because we could easily discern the buckle of the bracings for the first story. In the second test, with a PGA of 300 Gal, the residual drift ratio for the first story reached 4.22%, which is close to 5.33%. The remaining estimated post-earthquake seismic capacity was only 91.3 Gal after the test. The structure collapsed in the subsequent test.

For specimen *D*, which is identical to specimen *C*, we obtained the results after earthquake excitation with a PGA of 250 Gal (Table 6). The damage state was just slightly larger than that of specimen *C* after Test No. 2, with a PGA of 200 Gal. The estimated post-earthquake seismic capacity was 247.7 Gal. The structure collapsed in the subsequent test, with a PGA of 350 Gal. We again reached the conclusion that the estimated post-earthquake seismic capacities of specimens *C* and *D* were quite reasonable.

Table 6 Results of specimen D after earthqake excitation

No. of tests	Excited PGA (Gal)	Estimated seismic capacity A_p^D (Gal)	Residual seismic capacity ratio R_c (%)	Residual stiffness ratio R_k (%)	Residual drift ratio for the first story Δ_{res}^{1st} (%)	Residual drift ratio for the roof Δ_{res}^{roof} (%)	Residual lateral displacement of bracing (cm)	Observed damage level
1	250	247.7	95.4	48.2	0.31	0.04	3.80	Moderate
2	350				Collapse			

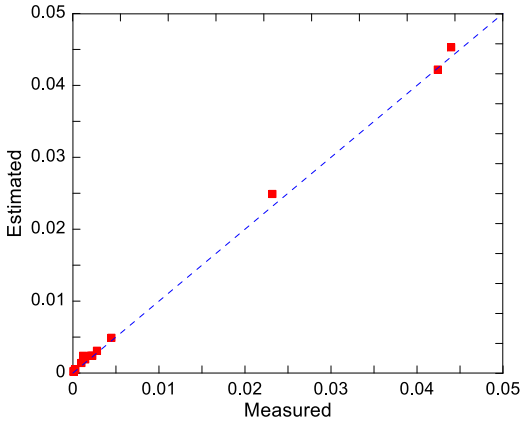

Fig. 10 The comparison of the measured and estimated residual drift ratios

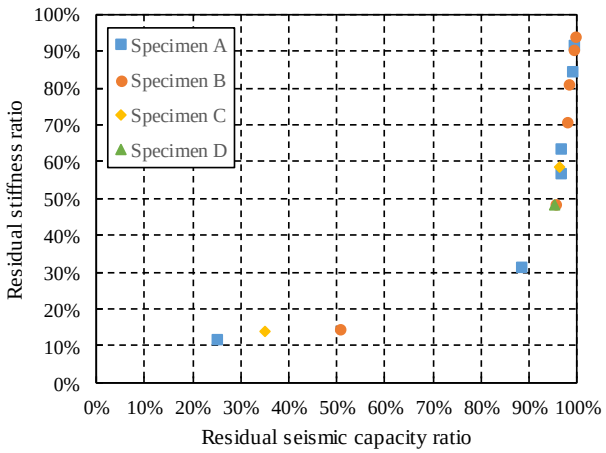

Fig. 11 Residual stiffness ratios and estimated residual seismic capacity ratios of the 4 specimens

In order to understand the accuracy of the residual drift ratio estimated using the proposed method, the measured and estimated residual drift ratios of the first story of all the tests in the four cases are plotted in Fig. 10. The Pearson correlation coefficient of these data is 0.9995. It is evident that the estimated residual drift ratios were quite close to the true value.

The results of the residual stiffness ratios and estimated residual seismic capacity ratios of the 4 specimens after each earthquake excitation are plotted in Fig. 11. The figure shows that even the residual stiffness ratio decreased to only approximately 30%, and the estimated residual seismic capacity still held at approximately 90%. However, it decreased dramatically when the residual stiffness ratio dipped below approximately 15%. The results of the residual drift ratios as well as the estimated residual seismic capacity ratios of the 4 specimens after each earthquake

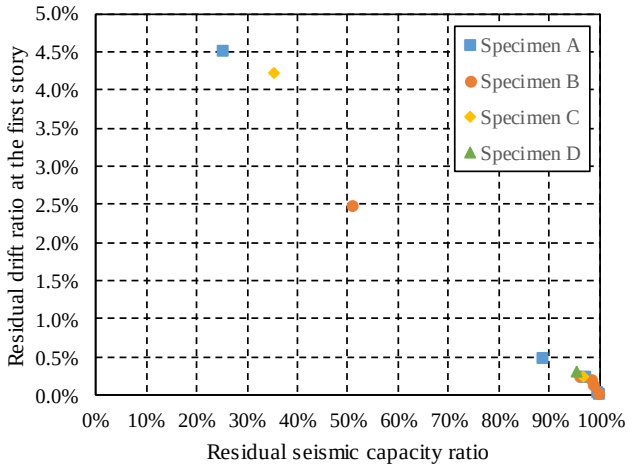

Fig. 12 Residual drift ratios of the first story and the estimated residual seismic capacity ratios of the 4 specimens

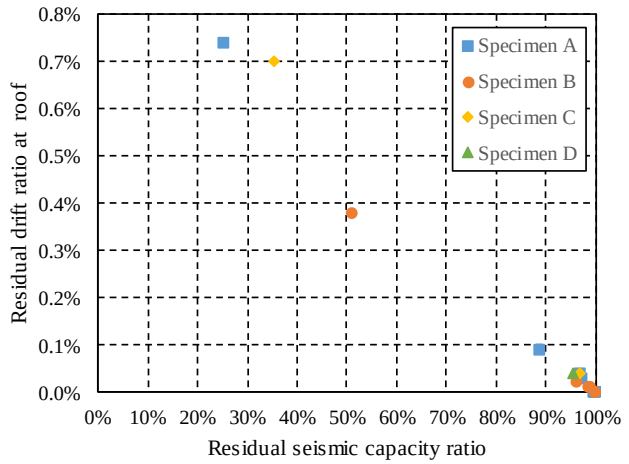

Fig. 13 Residual drift ratios of the roof and the estimated residual seismic capacity ratios of the 4 specimens

excitation for the first story and for the roof are plotted in Figs. 12 and 13, respectively. Observing Figs. 12 and 13, it is evident that the relationship between the residual drift ratios and the residual seismic capacity ratio is quite linear. Since the sensitivities between the residual drift ratios and the residual seismic capacity were consistent through the whole range of the residual drift ratios, it is easy to estimate the residual seismic capacity using the measured residual drift ratios. On the other hand, the sensitivity between the residual stiffness ratio and the residual drift ratios is too sensitive when the residual stiffness ratio is low. Therefore, compared to the residual stiffness ratio, it is easier to use residual drift ratios to estimate the residual seismic capacity of a building.

5. Conclusions

For this study, we used the measured relative displacement and absolute acceleration of the building response during an earthquake to estimate the post-earthquake seismic capacity. We used the curve-fitting approach to extract the normalized residual stiffness and the maximum residual roof displacement after an earthquake excitation from the hysteretic diagram of the normalized base shear and relative roof displacement. The post-earthquake capacity curve was obtained by updating a known capacity curve of the intact structure, using the normalized residual stiffness and the maximum residual roof displacement. The seismic capacities of the structure both before and after an earthquake were estimated using the modified CSM. Four small-scale specimens of the 6-story building were constructed and tested on the shaking table of the NCREE by using earthquake excitation with incremental PGA. We observed that when the PGA of the earthquake was smaller than the estimated seismic capacity in PGA, the reduction in estimated seismic capacity of the specimens post-excitation was relatively small (approximately higher than 88%), even after several excitations. Conversely, when the PGA of the earthquake was larger than or approximately equal to the estimated seismic capacity in PGA, the specimens suffered extensive damage (with an estimated residual seismic capacity ratio below 50%), or they collapsed. We conclude that by using the proposed approach, the post-earthquake seismic capacity can be estimated in a straightforward and reasonable manner. Note that because the proposed method employs the pushover analysis, the building type not suitable for the pushover analysis is not applicable to the proposed method. Hence, if the modal participating mass ratio of the first mode is not high enough, the building is not suitable for the proposed method. Besides, it should also be noted that because the proposed method is mainly based on the CSM method, it may not always obtain conservative results for engineering practice.

The proposed approach is applicable only to structures with a capacity curve that can be determined from nonlinear pushover analysis. In other words, the structures must meet this condition for this approach to be applied successfully. Because of the massive loss of public buildings such as schools, police stations, and district office buildings during earthquakes, many seismic evaluations such as nonlinear static pushover analysis have already been conducted to assess such structures. Therefore, many buildings are available for analysis. In addition, the relative displacement and absolute acceleration of the building response of each story necessitate simultaneous measurements with an acceptable degree of accuracy to obtain the hysteretic diagram of the roof displacement and base shear during an earthquake. In practice, although not popular yet, there is at least one real building in Tokyo, Japan with measurement of displacement response (Shiraishi and Okada 2009). The inter-story drift displacement of the building was measured during the 2007 Chūetsu offshore earthquake. Hopefully, economically viable smart sensors are becoming readily available for large-scale installation on structures because of the rapid development of sensor technology over the last decade. Moreover, the stockholders of such structures are becoming aware of the importance of rapid recovery after frequently occurring small and moderate earthquakes to mitigate economic loss, especially when concerning structures that have a high economic value such as high-tech factories as well as financial centers. Therefore, we believe more structures will increasingly be subject to pre-earthquake seismic evaluations and be equipped with adequate sensing systems to prepare for improved earthquake resilience in the future.

Acknowledgements

This research was supported in part by the Taiwan's Ministry of Science and Technology under the grant No MOST106-2622-M-011-002-CC2. This work was also financially supported by the Taiwan Building Technology Center from The Featured Areas Research Center Program within the framework of the Higher Education Sprout Project by the Ministry of Education in Taiwan.

Reference

ASCE (2007), Seismic Rehabilitation of Existing Buildings, American Society of Civil Engineers, Reston, Virginia, United States.

ATC-40 (1996), Seismic Evaluation and Retrofit of Concrete Buildings, Applied Technology Council, Redwood City, California.

CPAMI (2011), Seismic Design Code for Buildings in Taiwan, Construction and Planning Agency Ministry of The Interior, Taipei, Taiwan. (in Chinese)

Dai, K., Wang, J., Li, B. and Hong, H.P. (2017), "Use of residual drift for post-earthquake damage assessment of RC buildings", *Eng. Struct.*, **147**, 242-255. https://doi.org/10.1016/j.engstruct.2017.06.001.

Dunand, F., Ait Meziane, Y., Gueguen, P., Chatelain, J.L., Guillier, B., Ben Salem, R., Hadid, M., Hellel, M., Kibboua, A., Laouami, N., Machane, D., Mezouer, N., Nour, A., Oubaiche, E. and Remas, A (2004), "Utilisation du bruit de fond pour l'analyse des dommages des bâtiments de Boumerdes suite au séisme du 21 mai 2003", *Memoires du Service Geologique de L'Algerie*, **12**, 177-191. (in French)

FEMA (2015), Hazus-MH 2.1: Technical Manual, Federal Emergency Management Agency, Washington, D.C., USA.

FEMA 273 (1997), NEHRP Guidelines for the Seismic Rehabilitation of Buildings, Federal Emergency Management Agency, Washington, D.C., USA.

FEMA 356 (2000), Prestandard and Commentary for the Seismic Rehabilitation of Buildings, Federal Emergency Management Agency, Washington, D.C., USA.

Hsiao, F.P., Oktavianus, Y., Ou, Y.C., Luu, C.H. and Hwang, S.J. (2016), "A pushover seismic analysis and retrofitting method applied to low-rise RC school buildings", *Adv. Struct. Eng.*, **18**(3), 311-324. https://doi.org/10.1260/1369-4332.18.3.311.

Kostinakis, K. and Morfidis, K. (2017), "The impact of successive earthquakes on the seismic damage of multistorey 3D R/C buildings", *Earthq. Struct.*, **12**(1), 1-12. https://doi.org/10.12989/eas.2017.12.1.001.

Li, R., Ge, H. and Maruyama, R. (2017), "Assessment of post-earthquake serviceability for steel arch bridges with seismic dampers considering mainshock-aftershock sequences", *Earthq. Struct.*, **13**(2), 137-150.

https://doi.org/10.12989/eas.2017.13.2.137.
Lin, B.Z. and Tsai, K.C. (2003), "Development of an object-oriented nonlinear static and dynamic 3D structural analysis program", Report No. CEER/R92-04, National Taiwan University, Taipei, Taiwan.
Lin, B.Z., Chuang, M.C. and Tsai, K.C. (2009), "Object-oriented development and application of a nonlinear structural analysis framework", *Adv. Eng. Softw.*, **40**(1), 66-82. https://doi.org/10.1016/j.advengsoft.2008.03.012.
Naeim, F., Hagie, S., Alimoradi, A. and Miranda, E. (2005), "Automated post-earthquake damage assessment and safety evaluation of instrumented buildings", JAMA Report No. 2005-10639, John A. Martin & Associates, Inc., Los Angeles, CA.
National Research Council (2011), National Earthquake Resilience: Research, Implementation, and Outreach, The National Academies Press, Washington, D.C., USA.
Ozer, E. and Soyoz, S. (2013), "Vibration-based damage detection and seismic performance assessment of bridges", *Earthq. Spectra*, **31**(1), 137-157. https://doi.org/10.1193/080612EQS255M.
Reuland, Y., Lestuzzi, P. and Smith, I.F. (2019), "Measurement-based support for post-earthquake assessment of buildings", *Struct. Infrastr. Eng.*, **15**(5), 647-662. https://doi.org/10.1080/15732479.2019.1569071.
Ruiz-García, J. and Aguilar, J.D. (2014), "Aftershock seismic assessment taking into account postmainshock residual drifts", *Earthq. Eng. Struct. Dyn.*, **44**(9), 1391-1407. https://doi.org/10.1002/eqe.2523.
Shiraishi, M. and Okada, K. (2009), "Structural health monitoring of buildings", *Constr. Constr. Plan.*, **708**, 58-63. (in Japanese)
Sung, Y.C. (2003), "Performance-based seismic evaluation and design of bridges", Ph.D. Dissertation, National Taiwan University, Taipei, Taiwan. (in Chinese)
Sung, Y.C., Su, C.K., Wu, C.W. and Tsai, I.C. (2006), "Performance-based damage assessment of low-rise reinforced concrete buildings", *J. Chin. Inst. Eng.*, **29**(1), 51-62. https://doi.org/10.1080/02533839.2006.9671098.
Tang, Z., Xie, X. and Wang, T. (2016), "Residual seismic performance of steel bridges under earthquake sequence", *Earthq. Struct.*, **11**(4), 649-664. http://dx.doi.org/10.12989/eas.2016.11.4.649.

KT